Particle characterization using multiple scattering decorrelation methods: Hard-sphere model system

Andreas Heymann, Christian Sinn,* and Thomas Palberg
Institut für Physik der Johannes-Gutenberg-Universität, Mainz, Germany
(Received 12 October 1999)

Applying static light scattering experiments, we characterize colloidal particles that are used as model hard-sphere systems in experiments investigating their crystallization kinetics. The particles comprise of a compact core of poly(methyl methacrylate) and short polymer hairs grafted onto the surface. We use a contrast variation procedure to determine the refractive index variation within the particles and observe that one component of the binary mixture used as a solvent penetrates the particles and masks completely the small polymer hairs. Making use of the determined refractive index variation, we obtain the average particle radius and its polydispersity from measurements of the particle form factor close to its minimae. The scattered intensity has been corrected carefully for multiple scattering contributions applying dynamic light scattering measurements with multiple scattering decorrelation. We obtain a mean particle radius of $\overline{R}=435\pm4$ nm and a polydispersity of $\sigma=2.5\%$, a resolution that has not been achieved with light scattering experiments before.

PACS number(s): 82.70.Dd, 06.30.Bp, 78.35.+c

I. INTRODUCTION

Colloidal suspensions of particles with a pair-interaction potential resembling very closely that of ideal hard spheres are of strong interest for fundamental research [1]. Colloidal hard sphere suspensions have been successfully applied as model systems in several studies dedicated to the phase behavior of condensed matter [2], e.g., in the investigation of crystallization kinetics [3,4,5,6,7]. They play a key role in the debate of whether mode-coupling theory is well suited for the description of the glass transition [8,9] and were used in investigations of the influence of fluid structure on rheological behavior [10,11].

For these investigations, it is crucial to know the radius of the particles under study with high accuracy. In addition, it has become clear recently from computer simulation studies that the particle size polydispersity has a strong influence on the phase boundaries. Bolhuis and Kofke [12] report a strong increase of the freezing and melting concentration, respectively, with increasing polydispersity, whereas Phan *et al.* [13] observe an effect of polydispersity upon the crystalline packing fraction, thereby altering the equation of state indirectly. Bartlett and Warren [14] report even reentrant melting of the crystalline phase for suspensions with considerable polydispersity.

A hard-sphere interaction potential of colloidal particles is generally obtained by grafting short hairs of polymers onto the rigid particle surface, for which the surrounding fluid is a good solvent. When the hairy layers of two particles approach each other, a steep repulsion results due to the free energy of solvation. Besides this, a nearly perfect match of the refractive indices of the particle core and the solvent strongly reduces the van der Waals attraction, as the terms in the optical spectral region, which are dominant for nonaqueous solvents, become negligible. Different approaches have been used to prove that the colloidal systems under study exhibit the wanted hard-sphere behavior [11,15].

The present investigation is dedicated to core-shell particles as described before, which we have used for the investigation of crystallization kinetics [6,7,16]. As mentioned, it is essential for these experiments to determine the particle size and polydispersity very accurately, which has to be performed *in situ*, as the removal of the suspending liquid would at least lead to a collapse of the polymer hairs on the particle surface. Different methods have been applied for this task, e.g., the analytical ultracentrifuge [17] or single-colloidal-particle tracking [18]. In the present contribution, we measure the particle form factor with static light scattering (SLS) experiments with high accuracy, applying a contrast variation procedure.

Contrast variation is very common for x-ray and neutron scattering investigations [19], where, e.g., the contrast can be reverted by the exchange of hydrogen with deuterium. In the optical region, however, contrast variation is considerably less frequently applied, because it usually implies the exchange of the solvent, which may strongly influence the system under investigation. In addition, for concentrated systems, multiple scattering contributions come readily into play, which can almost always be neglected in x-ray or neutron scattering studies. A feasible possibility for optical investigations is to suspend the particles in a binary solvent mixture, the composition of which can be altered. This method has been successfully applied by Philipse *et al.* [20] for the characterization of coated silica spheres. Information about the particle structure may be obtained with this procedure even if the particles are small compared with the wavelength of the incident radiation and correspondingly scatter spatially isotropically [21].

An accurate determination of the particle polydispersity

*Author to whom correspondence should be addressed.
Email address: Christian.Sinn@uni-mainz.de; URL: http://kolloid.physik.uni-mainz.de/

from SLS, however, requires a measurement of the particle form factor close to its minimae, where the scattered light intensity is dominated by multiple scattering. Fortunately, modern techniques for the decorrelation of multiple scattering in dynamic light scattering (DLS) [22,23,24] enable also a correction of the particle form factor for multiple scattering effects [6,25]. In the first part of our investigations, we described the application of multiple scattering decorrelation for particle sizing [26].

In this paper, we take advantage of a combination of both techniques, i.e., contrast variation and multiple scattering decorrelation, and apply a two-step procedure. We first determine the refractive index variation within the particles from SLS data that were obtained far off the zeros of the particle form factor. Three different solvent compositions are used for contrast variation. Subsequently, we repeat the analysis applying the determined refractive index variation and using all available data, corrected for multiple scattering. From this second step, we determine the final particle radius and the size polydispersity. This two-step procedure allows for an unrivaled precision in the determination of the particle polydispersity.

The paper is organized as follows. We shall first summarize the formulas we need for the evaluation of our measurements. This will be followed by a description of the experimental procedure. We then shall describe the results for the refractive index variation within the particles, their radius, and its polydispersity, and finish with a concluding discussion.

II. THEORETICAL CONSIDERATIONS

A. Form factor of core-shell particles and contrast variation procedure

The light scattered by a colloidal suspension of identical, rigid, and spherical particles can be generally described by

$$I(q)=I_0 N|b(0)|^2 P(q)S(q), \tag{1}$$

where I_0 is an optical constant, N is the number of particles in the scattering volume, and $q=(4\pi n_M/\lambda)\sin(\theta/2)$ is (the modulus of) the scattering vector at scattering angle θ; n_M is the refractive index of the suspending medium and λ is the wavelength of the light source in vacuum. $P(q)=|b(q)/b(0)|^2$ is the form factor of the particles, whereas $S(q)$ is the structure factor of the suspension, which comprises of the interparticle interference of light. In what follows, we assume noninteracting particles, that is $S(q)=1$:

$$b(q)=\int [n(r)-n_M]\exp(i\vec{q}\cdot\vec{r})d^3r \tag{2}$$

is the scattering amplitude of a single particle. The integration is performed over the volume of the particle, which may be optical inhomogeneous. We here restrict ourselves to refractive index variations $n(r)$ of spherical symmetry. If the integration is performed for an optically homogeneous particle, the well-known Debye form factor results

$$P(q)=\frac{9}{(qR)^6}(\sin qR-qR\cos qR)^2, \tag{3}$$

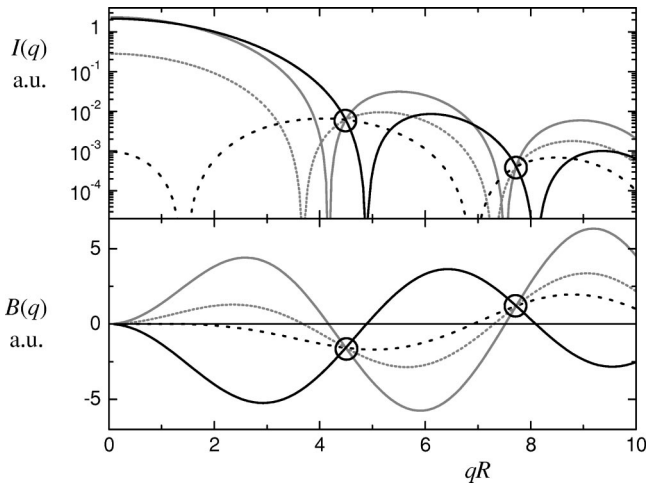

FIG. 1. Variation of the form factor $P(q)$ of a core-shell particle with the refractive index of the suspension medium, n_M. The thickness of the shell, d, and the refractive index of core and shell, n_0 and n_R, respectively, are kept constant. $I(q)\propto P(q)$ denotes the scattered intensity, whereas $B(q)\propto b(q)q^2$ (both plotted in arbitrary units). Dark solid curve, $n_M>n_0$; dark broken curve, $n_M\approx n_0$; light broken curve, $n_M=n_0$; light solid curve, $n_M<n_0$.

with R the radius of the sphere and

$$b(0)=\frac{4\pi}{3}R^3(n-n_M). \tag{4}$$

In this contribution, we are concerned with inhomogeneous spheres, the form factor of which may be conveniently expressed by using dimensionless profiles $\nu(r)$ as follows:

$$n(r)-n_M=(n_0-n_M)\nu_e(r)+(n_R-n_0)\nu_i(r). \tag{5}$$

ν_e denotes the cutoff from the external shape of the particle, i.e., $\nu_e=0\,\forall r>R$ and $\nu_e=1\ \forall\leqslant R$, whereas ν_i describes the variation of the refractive index within the particle. As before, n_M is the refractive index of the surrounding medium, $n_R=n(r=R)$ is the refractive index at the particle surface, and $n_0=n(r=0)$ is the refractive index at the center of the particle. For a core-shell particle with the shell thickness d, we have $\nu_i=0\,\forall R<r\leqslant R-d$ and $\nu_i=1\,\forall R-d<r\leqslant R$. We note that ν_i may also be chosen to be a continuous variable. For future convenience, we define a scattering strength $B(q)=q^2b(q)/4\pi$, for which one obtains for core-shell particles

$$\begin{aligned}B(q)q=&(n_0-n_M)[\sin qR-qR\cos qR]\\&+(n_R-n_0)[\sin qR-qR\cos qR-\sin(qR-qd)\\&+(qR-qd)\cos(qR-qd)].\end{aligned} \tag{6}$$

The form factor for a given particle with fixed n_0 and n_R changes significantly with the refractive index of the solvent n_M as described by Eq. (6). Corresponding calculations are shown in Fig. 1 for $I(q)\propto B(q)^2/q^4$ and $B(q)$. Two isoscattering points are indicated by circles; these reflect the scattering from the shell only, where the contrast is with respect to the core, which is unchanged upon varying the refractive index of the solvent. The numerical advantage of fitting $B(q)$

to experimental data is a reduction of their dynamic range as compared with $b(q)$. For the reader's convenience, we note that $B(K)$ in Ref. [20] equals our $b(q)$.

B. Polydispersity

Up to now, the scattered light has been assumed to originate from N identical particles with form factor $P(q)$ each. However, every colloidal sample exhibits a certain amount of polydispersity, meaning that the particle radii are distributed about the mean radius $\overline{R}$ with a significant spread. In this case, the scattered intensity $I_{\mathrm{poly}}(q)$ can be obtained from

$$I_{\mathrm{poly}}(q,\overline{R},s)=N\int_0^\infty I_{\mathrm{mono}}(q,R)p(R,\overline{R},s)dR, \tag{7}$$

where $I_{\mathrm{mono}}(q,R)$ describes the scattered intensity from a single particle with radius R. $p(R,\overline{R},s)dR$ denotes the probability to find an individual particle radius R and depends on the mean radius $\overline{R}$ and the width s of the distribution; even further parameters may be needed to describe the distribution completely. A reliable method for the determination of arbitrary particle size distributions has been demonstrated by Schnablegger and Glatter [27]. We note that approaches using Eq. (7) neglect optical polydispersity, i.e., the refractive index variation $n(r)$ is independent from the particle size.

An analytical solution [28] of Eq. (7) using Eq. (3) is known for the unimodal gamma or Schulz [29] distribution,

$$p(R,\overline{R},\sigma)=\frac{\exp(-\alpha R/\overline{R})}{(\overline{R}\sigma^2)^{\alpha}\Gamma(\alpha)}R^{\alpha-1}$$

$$\text{with}\quad \alpha=\sigma^{-2};\quad \sigma=s/\overline{R}. \tag{8}$$

The result reads in our notation

$$P(x,\sigma)=\frac{9\Gamma(\alpha)}{2x^6\sigma^{12}\Gamma(\alpha+6)}\{[1-C\cos X]-2xC^{1+\sigma^2}\times\sin(X+X\sigma^2)+x^2(1+\sigma^2)[1+C^{1+2\sigma^2}\times\cos(X+2X\sigma^2)]\}, \tag{9}$$

where $x=q\overline{R}$, $X=\alpha\arctan(2x\sigma^2)$, and $C=(1+4x^2\sigma^4)^{-\alpha/2}$; $b(0)=(4\pi\overline{R}^3/3)(n-n_M)$.

Equation (9) is drawn in Fig. 2 using three different polydispersity indices σ. A finite polydispersity manifests itself not only in finite scattering intensity at the zeros of the form factor for monodisperse suspensions, but also by an increasing shift of the minimae of the scattered intensity with increasing polydispersity. We note without proof that the same is true for inhomogeneous spheres.

We use Eq. (9) in this contribution for reference purposes only, because it is already complicated to fit to experimental data for homogeneous spheres. For our inhomogeneous spheres, we approximate size polydispersity by a simple trimodal distribution according to

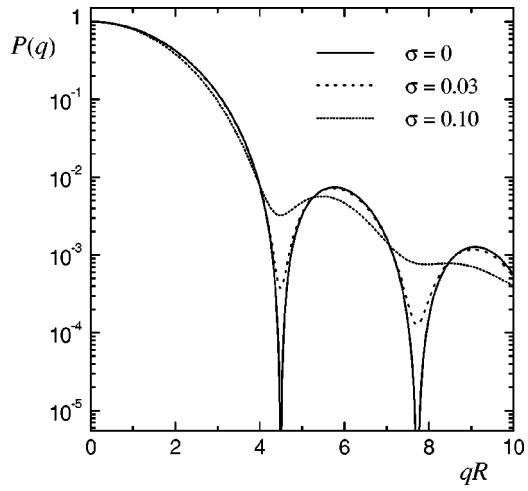

FIG. 2. Particle form factor $P(q)$ as a function of qR. Parameter is the polydispersity index σ. The curves are calculated from Eq. (9).

$$p(R,\overline{R},s)=C\,\delta[\overline{R}-s]+(1-2C)\,\delta[\overline{R}]+C\,\delta[\overline{R}+s]. \tag{10}$$

The undetermined constants $\overline{R}$, C, and s are chosen such that the moments of this discrete distribution equal those of a Gaussian. From symmetry, it is obvious that both means are identical. Equating the second moments yields $s^2/\overline{R}^2=\sigma^2/2C$, where $\sigma\overline{R}$ is the standard deviation of the Gaussian distribution. Finally, we obtain from the forth moments $C=\frac{1}{6}$, and correspondingly

$$I_{\mathrm{poly}}(q,\overline{R},\sigma)=\frac{1}{6}NI_{\mathrm{mono}}(q,\overline{R}-\sqrt{3}\sigma\overline{R})+\frac{2}{3}NI_{\mathrm{mono}}(q,\overline{R})+\frac{1}{6}NI_{\mathrm{mono}}(q,\overline{R}+\sqrt{3}\sigma\overline{R}), \tag{11}$$

which is used in our fits. Calculations for homogeneous spheres show that Eq. (11) does not significantly differ from the exact result, Eq. (9), for polydispersity indices σ below approximately 5%. The use of this simplified formula enables us to take into account an arbitrary refractive index variation that has not been specified *a priori*.

III. EXPERIMENTAL DETAILS

A. Sample preparation

In this contribution, we employ particles that have been synthesized by Underwood *et al.* [30] (SMU28). They are comprised of a core of poly(methyl methacrylate) (PMMA) with approximately $R=440$ nm, onto which chains of poly-(hydroxy stearic acid) (PHSA) are grafted by a chemical process [31]. These chains have a length of approximately 10 nm [11]. As an index-matching solvent, we use a suitable chosen mixture of decahydro-naphthalene (DHN, isomeric mixture) and 1,2,3,4-tetrahydro-naphthalene (THN), both supplied by Merck, Germany. The index match point is located at approximately 35% THN content by volume.

The samples in this study are simply prepared by mixing a suitable volume THN (V_T) with DHN (V_D). We use Φ_T

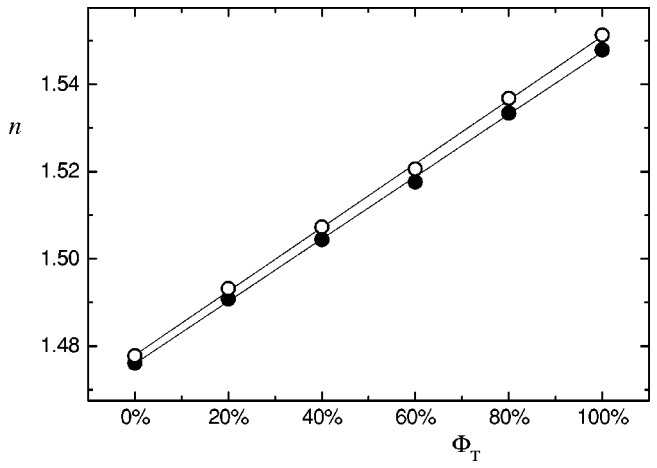

FIG. 3. Refractive index of different DHN/THN mixtures as a function of composition Φ_T, the volume fraction of THN. Measurements were performed at $\lambda = 488\,\mathrm{nm}$ (open dots) and $\lambda = 515\,\mathrm{nm}$ (solid dots). Drawn lines are linear fits.

$= V_T/(V_D+V_T)$ as the specification of THN concentration. Note that the denominator may deviate from the total volume after mixing. A few drops of a suspension of the particles in DHN are subsequently added to the solvent mixture. The measurements in this investigation were all performed at particle volume fractions $\phi = 0.05-0.5\,\%$.

Figure 3 shows the refractive index of the solvent mixture as a function of THN content Φ_T at two different wavelengths. The data were obtained using an Abbe refractometer without an Amici direct-sight prism. The white-light source was equipped with suitable interference filters ($\Delta\lambda = 5\,\mathrm{nm}$). From these data, we determine n_M, which is fixed in the fitting procedure described subsequently.

B. Decorrelation of multiple scattering

In this contribution, we take advantage of the two-color cross-correlation scheme for the suppression of multiple scattering, which has been already described in detail [22,23]. Therefore, we give here only a concise description of its working principle. Multiple scattering contributions to temporal correlation functions can be decorrelated by cross correlating the temporal fluctuations of two simultaneously performed, geometrically different scattering experiments that share a common wave vector $\vec{q}$ and the same scattering volume. Details may be found in Ref. [32]. In the case of the two-color scheme, the independent experiments are realized by two different laser wavelengths and a narrow bandwidth filter in front of the respective detector. Usually, a multiline Ar^+ laser is employed, using the main $\lambda = 488.0\,\mathrm{nm}$ and $\lambda = 514.5\,\mathrm{nm}$ wavelengths. The results we report here were obtained with the original setup in Kiel [22]. There, a Köster prism with a dichroic layer was used to separate the incident wavelengths, which has been replaced by a dispersion prism in contemporary setups owing to difficulties with the dichroic layer [23]. Our results, however, are not prone to these problems. The cross-correlation functions were recorded using the ALV-5000 correlator.

The normalized intensity cross-correlation function $g_{12}(\tau)$ can be written in the homodyne limit as

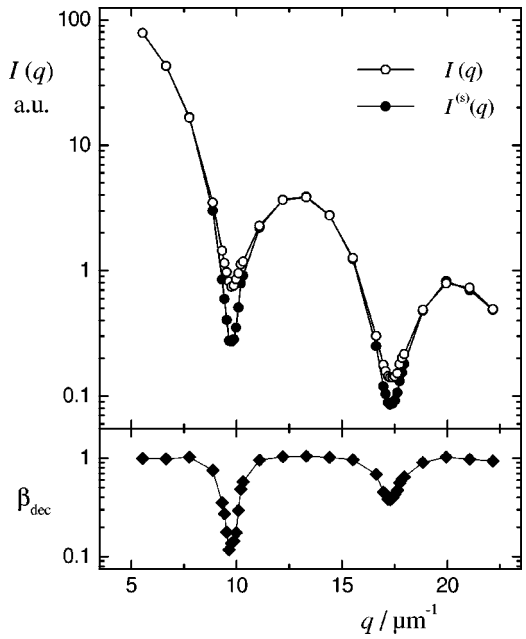

FIG. 4. Demonstration of static light scattering correction for multiple scattering contributions. (a) Top, $I(q)$, measured intensity data, which contain multiple scattering contributions. $I^{(s)}(q)$, singly scattered light intensity as obtained by the correction procedure described in the text. (b) Bottom, β_{dec}, squared ratio of singly to totally scattered light as obtained from a dynamic light scattering experiment. The sample volume fraction was $\phi = 5\times10^{-4}$, the solvent was pure DHN ($\Phi_T = 0$). Drawn lines are guides to the eye.

$$g_{12}(\tau) = \frac{\langle I_1(0) I_2(\tau)\rangle}{\langle I_1\rangle\langle I_2\rangle} = 1 + \beta_{\mathrm{dec}}\beta_{\mathrm{opt}}(q)\,|f(q,\tau)|^2, \quad (12)$$

where $\beta_{\mathrm{dec}}\beta_{\mathrm{opt}}$ is the intercept of the cross-correlation function. $f(q,\tau)$ is the so-called intermediate scattering function and represents the sample fluctuations. If a monodisperse suspension of spheres is assumed, $f(q,\tau) = \exp(-Dq^2\tau)$, where D is the diffusion coefficient of the colloidal spheres. The intercept is given by a product of two contributions. β_{dec} is the ratio of singly to total scattered light intensity, that is $\beta_{\mathrm{dec}} = (I_1^{(s)} I_2^{(s)})/(I_1 I_2)$; the subscripts denote the different detectors. β_{opt} is an apparatus constant, which is, unfortunately, an unknown function of q in the case of the dual-color experiment [23]. The angular variation of $\beta_{\mathrm{opt}}(q)$ has to be measured, therefore, with the aid of a reference sample. Hence, the singly scattered light intensity is obtained as

$$I^{(s)}(q) = [I(q)/I_{\mathrm{ref}}][\beta_{\mathrm{dec}}\beta_{\mathrm{opt}}(q)/\beta_{\mathrm{ref}}(q)]^{1/2}. \quad (13)$$

As reference, we use a dilute sample of polystyrene latex spheres of radius $R = 12\,\mathrm{nm}$. This sample can be assumed to exhibit no multiple scattering ($\beta_{\mathrm{dec}} = 1$). In addition, its form factor is angularly independent, leading to an angularly invariant light scattering intensity I_{ref} that is used to correct for small misalignments of the apparatus. $\beta_{\mathrm{dec}}\beta_{\mathrm{opt}}(q)$ is determined from the extrapolation $g_{12}(\tau\to0)$ using a single-exponential approximation for $f(q,\tau)$.

The procedure is exemplarily shown in Fig. 4. In Fig. 4(a) experimental points are shown without and with correction for multiple scattering using Eq. (13), denoted $I(q)$ and

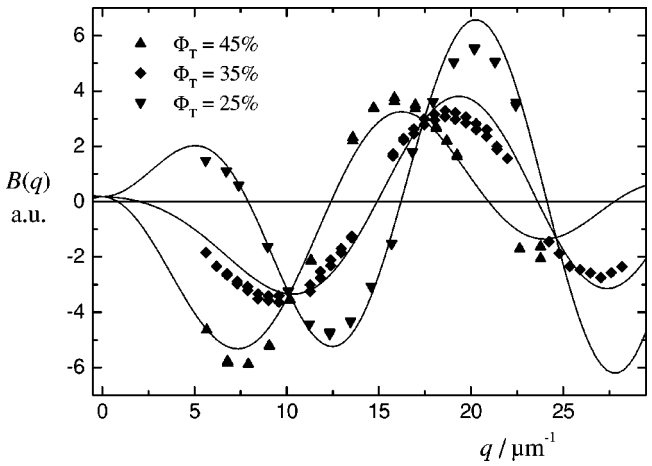

FIG. 5. Contrast variation method for the determination of the refractive index variation within the particle. The scattered field $B(q)$ is determined for three different compositions of the suspending medium $\Phi_T=\{0.25,0.35,0.45\}$. The solid curves are obtained by a global fit to the data according to the linear refractive index variation of Eq. (14). Note that the data close to the zeros are omitted. For details see text.

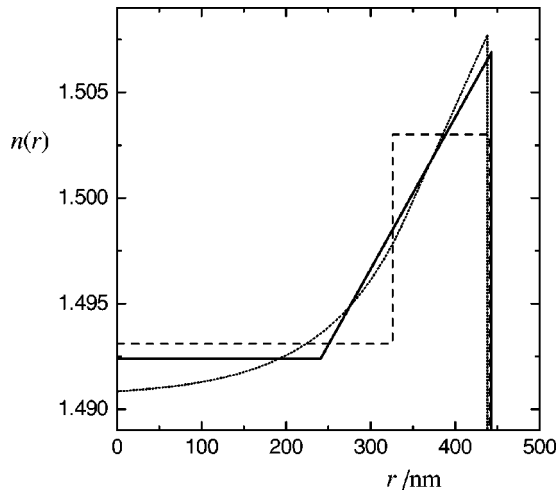

FIG. 6. Radial variation of the refractive index $n(r)$ within an individual particle, as obtained from the fitting procedure as described in the text. Dashed curve, step function ($\chi^2=123$); dotted curve, diffusion model ($\chi^2=26$); solid curve, linear model ($\chi^2=37$) as used for the final results.

$I^{(s)}(q)$ respectively. Figure 4(b) shows β_{dec} that is used to correct for multiple scattering present in Fig. 4(a). We note that we use the q scale corresponding to $\lambda=514.5\,\mathrm{nm}$. If σ would be determined from the first form factor minimum of $I(q)$, a value of $\sigma=4.2\%$ resulted, as compared to $\sigma=2.5\%$ determined from $I^{(s)}(q)$ (see below). This illustrates the importance of multiple scattering corrections for the determination of small particle polydispersities.

In the subsequent evaluation, we further correct the intensity data for sedimentation during the measurements, which may last up to two days. In addition, we normalize the data by the particle volume fraction, which is necessary in order to fully exploit the contrast variation technique.

IV. RESULTS AND DISCUSSION

A. Variation of the refractive index within the particles

The scattered intensity corrected for multiple scattering contributions as a function of q was determined using three different THN concentrations: below ($\Phi_T=0.25$, $n_M=1.4939$), above ($\Phi_T=0.45$, $n_M=1.5081$), and approximately at the index match point ($\Phi_T=0.35$, $n_M=1.5010$), respectively. In what follows, we fit these three data sets simultaneously, i.e., we fix n_M at the experimentally determined value and choose the remaining parameters such that they describe the three data sets equally well.

First, we determined the refractive index variation within the particles. We already mentioned that the data can be fitted more easily when the experimental intensity data are converted into $B(q)$. The sign ambiguity after taking the square root of the intensity is resolved by the following sign convention. We affix a positive sign to the data that belong to small q and low THN content. At the zeros, we change sign. The data obtained from this procedure are shown in Fig. 5. Note that data close to the zeros are omitted, as we intend to neglect polydispersity in this first step.

We expected to observe a step function for the refractive index variation, comprising of the compact PMMA core ($n\approx1.49$) and the thin PHSA layer ($n=1.476$). Accordingly, we choose a step function for ν_i and fitted the data shown in Fig. 5 to the form factor calculated correspondingly.

To our surprise, only a step function with a *higher* refractive index in the shell could reproduce our data. Note that this is already visible without fit from the isoscattering fixed points with our sign convention in mind. We interpret this observation by an imbibition of THN into the particle core, which rises the refractive index within a certain shell over the value of PMMA. This effect is similar to that observed for the same kind of particles in a binary mixture of DHN and CS_2 [33].

Having established a refractive index variation caused by the penetration of THN into the particle core, there is no reason for preferring the step function over competing variations. Accordingly, we fitted our data to a refractive index profile that is similar to that resulting by a solvent diffusion process into the particle. However, when we tried several different fitting functions, it turned out that the goodness of the fit depends mainly on the number of fit parameters and not on the chosen refractive index profile [6]. This means that we cannot specify a unique refractive index profile that describes the smooth decrease of the refractive index towards the particle core. For simplicity, we prefer to use the linear function

$$\nu_i=\begin{cases} 0 & \forall R<r\leqslant R-d \\ 1-\dfrac{R-r}{d} & \forall R-d<r\leqslant R. \end{cases} \tag{14}$$

A fit to the data shown in Fig. 5 yields the parameters $R=443\,\mathrm{nm}$, $d=202\,\mathrm{nm}$, $n_0=1.4924$, and $n_R=1.5069$. For comparison, a few of the modeling functions are shown in Fig. 6 with the χ^2 from the respective fit specified in arbitrary units. Note that the diffusion model and the linear variation fit the data equally well.

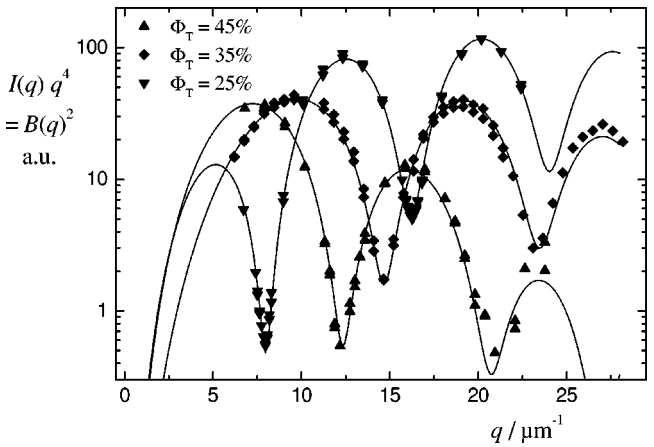

FIG. 7. Determination of the polydispersity. The scattered intensity $I(q)q^4 \propto B(q)^2$ is determined for three different compositions of the suspending medium $\Phi_T = \{0.25, 0.35, 0.45\}$. The solid curves are obtained by a global fit to the data. A trimodal particle distribution according to Eq. (11) has been assumed. In addition, the linear refractive index variation according to Eq. (14) has been used. In contrast to Fig. 5, every data point has been included in the analysis. For details see text.

This result indicates that the hairy layer, which is responsible for the hard-sphere behavior of the particles, does not contribute significantly to the static data owing to the overwhelming effect of the strong refractive index variation as a result of the penetration of THN into the particle core. In addition, it remains unclear whether this layer is visible at all in an optical experiment, as the thin hairs extend into a solvent of almost the same refractive index. There are, however, experiments reported where the hairy layer has been observed with expected extension [34,11].

We performed corresponding measurements with similar particles at a subsequent instants of time after their first exposure to THN. With a diffusive penetration kinetics and its square-root temporal behavior in mind, we can estimate a time constant of the order of $10^3\ \mu\text{m}^2$/day. Whereas this large time constant means that the particles are optical inhomogeneous over the whole experimental time scale (from 1 h to a few years), we conclude at the same time that our experiments were performed in a stationary regime. For a different approach, compare Ref. [11].

B. Particle radius and size polydispersity

Following the same line of data evaluation, we now include also the data close to the form factor minimae in the fit. Again, the data are globally fitted to the measured form factors for three different solvent compositions. For polydisperse systems $b(q)$ and correspondingly $B(q)$ cannot be defined unambiguously. We therefore use $I(q)q^4$ for the fitting procedure, which is proportional to $B(q)^2$ for a single particle. As there are no zeros left for polydisperse systems, intensity data suffice anyway.

We apply the trimodal particle radius distribution according to Eq. (11), which is used together with the linear refractive index variation as described in the preceding section for the calculation of the form factor. We take the parameters from the preceding section as start parameters, and release with every fitting step an additional fit parameter, until in the last step every fit parameter is varied. This procedure is necessary, because the fit is now delicate owing to the absence of sign changes in $B(q)$. The result is shown in Fig. 7. We obtain the following fit parameters: $\bar{R} = 435 \pm 4$ nm, $\sigma = 2.5\%$, $d = 213$ nm, $n_0 = 1.4941$, $n_R = 1.5064$.

This is our final result for the characterization of the particles under study. We note that the mean radius is slightly smaller than the one determined in the preceding section. This is easily understood, because the larger particles scatter stronger and dominate therefore in an evaluation, where polydispersity has not been accounted for.

The particle radius can be determined very sensitively from the position of the Bragg peaks of crystallizing samples. The sample concentration has been determined independently by sedimentation experiments following Paulin and Ackerson [15]. We obtained $R = 445 \pm 2$ nm [6], which agrees perfectly with the previous value taking into account the thin hairy layer of approximately 10 nm, which is invisible in SLS.

We also evaluated the cross-correlation functions obtained by DLS in order to obtain the particle radius. Unfortunately, we could not obtain agreement with the radii reported above. The result was $R \approx 460$ nm, a value that is significantly too high. The viscosity of mixtures of DHN and THN with different composition was determined independently using an capillary viscosimeter. However, DHN itself is a mixture of two isomeric species, the respective concentration of which is unknown and may vary from batch to batch. The viscosity of the pure DHN isomers differs by 50%. Thus, we attribute the lack of correspondence of the DLS and SLS data to the viscosity of the solvent, which has obviously not been determined with sufficient accuracy, a point which needs further clarification.

V. CONCLUDING REMARKS

In conclusion, we shall give some comments on the relation of the present contribution with earlier work dedicated to the measurement of polydispersities of colloidal suspensions by light scattering methods.

In extension to the thorough investigation by Philipse *et al.* [20], we could analyze our data to obtain the (small) polydispersity of our particles. This was only possible by correcting the light scattering data for multiple scattering contributions. In addition, with our method we do not rely on an *a priori* defined refractive index variation within the particles. Instead, we can even determine the refractive index variation independently.

The determination of small polydispersities from SLS presented here should be compared with the competing method by DLS, which has been used by Pusey and van Megen [35]. They determine the apparent radius of a colloidal sample by DLS as a function of q. Close to the particle form factor minimae, the apparent radius (or the inverse diffusion coefficient) exhibits a dispersionlike behavior. At small q, where the form factor of the larger particles is located, the measured radius is dominated by smaller particles, and vice versa. This way, the particle form factor scans the size distribution. The difference between minimal and maximal radius of the dispersionlike curve is $2s \approx 2\sigma\bar{R}$. In their paper, Pusey and van Megen demonstrate this method to

work with a suspension of index-matched PMMA particles very similar to ours, and obtained a polydispersity of $\sigma = 6\%$. No multiple scattering correction was applied to their data, which would be, however, a readily performed extension to their work.

We estimate the upper limit of their polydispersity determination to be comparable to ours. If the polydispersity almost completely washes out the modulation of the particle form factor, only a lower bound for the polydispersity can be determined. This may occur above $\sigma \approx 10\%$ (compare Fig. 2).

The lower limit of their method, however, differs from ours and is given by the accuracy of DLS linewidth measurements, which can be hardly better than $\pm 3\%$. Frequently, the measurements differ even by $\pm 5\%$ [26]. This fact limits the measurable polydispersity to $\sigma > 3\%$. Note that this is an optimistic view. If multiple scattering decorrelation is applied, the count rate in the form factor minimae might remain comparatively high, but the number of correlated counts become excessively low, thereby strongly reducing the intercept of the cross-correlation function and hence the accuracy.

The evaluation we performed in this contribution is not prone to these problems. The intensity correction is only needed with moderate accuracy, because the scattered intensity at the form factor minimae depends strongly on polydispersity (cf. Fig. 2). In addition, we fit several data points from different particle form factors simultaneously. Thereby, we estimate our lower limit of polydispersity resolution to approximately $\sigma = 1\%$.

In conclusion, we have fruitfully exploited the amount of information present in SLS data. The procedure we introduced in this contribution imposes no severe restrictions on the data quality and yields reliable values for small polydispersities, provided that the intensity data are carefully corrected for multiple scattering. Polydispersity is an important parameter as far as crystallization experiments are concerned. We determine a very small polydispersity of the particles we use, which strongly favors the use of these particles for crystallization experiments. On the other hand, we observe that the organic solvents slowly and selectively penetrate the particles, which has been reported already for a different solvent mixture. This effect has to be taken into account properly for precise optical investigations. The procedure we introduced here is capable to determine this time-dependent penetration of solvents into colloidal particles with high accuracy and may therefore be applied also to different systems.

ACKNOWLEDGMENTS

We gratefully acknowledge fruitful discussions concerning the topics of this paper with Norbert Garbow, Jürgen Müller, Ekkehard Overbeck, Andreas Stipp, and Claus Urban. The present investigations were initiated by late Klaus Schätzel, to whom we owe inspiring ideas and suggestions. We are grateful to Bill van Megen for the gift of the particles used in the present and related work. This work was financed by DFG project Scha389/4, SFB 262, and MWFZ.

[1] P. N. Pusey, in *Liquids, Freezing and Glass Transition*, Proceedings of the Les Houches Summer School, Les Houches, 1989, edited by J. P. Hansen, D. Levesque, and J. Zinn-Justin (North-Holland, Amsterdam, 1991), p. 763.
[2] P. Bartlett and W. van Megen, in *Granular Matter: An Interdisciplinary Approach*, edited by A. Mehta (Springer, New York, 1994), p. 195.
[3] K. Schätzel and B. J. Ackerson, Phys. Rev. E **48**, 3766 (1993).
[4] Y. He, B. J. Ackerson, W. van Megen, S. M. Underwood, and K. Schätzel, Phys. Rev. E **54**, 5286 (1996).
[5] J. L. Harland and W. van Megen, Phys. Rev. E **55**, 3054 (1997).
[6] A. Heymann, doctoral thesis, Christian-Albrechts-Universität zu Kiel, Kiel, 1997.
[7] A. Heymann, A. Stipp, C. Sinn, and T. Palberg, J. Colloid Interface Sci. **209**, 119 (1998).
[8] W. Götze and L. Sjögren, Phys. Rev. A **43**, 5442 (1991).
[9] W. van Megen and S. Underwood, Phys. Rev. E **49**, 4206 (1994).
[10] P. N. Segrè, S. P. Meeker, P. N. Pusey, and W. C. K. Poon, Phys. Rev. Lett. **75**, 958 (1995).
[11] S.-E. Phan, W. B. Russel, Z. Cheng, J. Zhu, P. M. Chaikin, J. H. Dunsmuir, and R. H. Ottewill, Phys. Rev. E **54**, 6633 (1996).
[12] P. G. Bolhuis and D. A. Kofke, Phys. Rev. E **54**, 634 (1996).
[13] S.-E. Phan, W. B. Russel, J. Zhu, and P. M. Chaikin, J. Chem. Phys. **108**, 9789 (1998).
[14] P. Bartlett and P. B. Warren, Phys. Rev. Lett. **82**, 1979 (1999).
[15] S. E. Paulin and B. J. Ackerson, Phys. Rev. Lett. **64**, 2663 (1990).
[16] A. Heymann, A. Stipp, C. Sinn, and T. Palberg (unpublished).
[17] W. Mächtle, G. Ley, and R. Rieger, Colloid Polym. Sci. **273**, 708 (1995).
[18] N. Garbow, J. Müller, and T. Palberg, Physica A **235**, 291 (1997).
[19] Compare, e.g., T. Kawaguchi, J. Appl. Crystallogr. **28**, 424 (1995); for a recent SAXS study: N. Dingenouts, Y. S. Kim, and M. Ballauff, Colloid Polym. Sci. **272**, 1380 (1994); for a recent SANS study: S. Egelhaaf, U. Olsson, P. Schurtenberger, J. Morris, and H. Wennerström, Phys. Rev. E **60**, 5681 (1999); a SANS study similar to the present investigation is by M. Gradzielski, D. Langevin, L. Magid, and R. Strey, J. Phys. Chem. **99**, 13 232 (1995).
[20] A. P. Philipse, C. Smits, and A. Vrij, J. Colloid Interface Sci. **129**, 335 (1989).
[21] J. Rička, M. Borkovec, and U. Hofmeier, J. Chem. Phys. **94**, 8503 (1991).
[22] M. Drewel, J. Ahrens, and U. Podschus, J. Opt. Soc. Am. A **7**, 206 (1990).
[23] P. N. Segrè, W. van Megen, P. N. Pusey, K. Schätzel, and W. Peters, J. Mod. Opt. **42**, 1929 (1995).
[24] E. Overbeck and C. Sinn, J. Mod. Opt. **46**, 303 (1999).
[25] C. Urban and P. Schurtenberger, J. Colloid Interface Sci. **207**, 150 (1998).

[26] C. Sinn, R. Niehüser, E. Overbeck, and T. Palberg, Part. Part. Syst. Charact. **16**, 95 (1999).
[27] H. Schnablegger and O. Glatter, J. Colloid Interface Sci. **158**, 228 (1993).
[28] S. R. Aragón and R. Pecora, J. Chem. Phys. **64**, 2395 (1976).
[29] G. V. Schulz, Z. Phys. Chem. Abt. B **43**, 25 (1935).
[30] S. M. Underwood, J. R. Taylor, and W. van Megen, Langmuir **10**, 3550 (1994).
[31] R. J. R. Cairns, R. H. Ottewill, D. W. S. Osmond, and I. Wagstaff, J. Colloid Interface Sci. **54**, 45 (1976).
[32] K. Schätzel, J. Mod. Opt. **38**, 1849 (1991).
[33] R. Ottewill and I. Livsey, Polymer **28**, 109 (1987).
[34] W. van Megen (private communication).
[35] P. N. Pusey and W. van Megen, J. Chem. Phys. **80**, 3513 (1984).